# Relationship between specific microRNA expression and radioresistant conditions in HL60 acute myeloid leukemia cells

HIKOTO SUGIYAMA[1], MEGUMI KIKUCHI[1], MITSURU CHIBA[2,3], YOICHIRO HOSOKAWA[1] and SATORU MONZEN[1,3]

[1]Department of Radiation Science, Hirosaki University Graduate School of Health Sciences, Hirosaki, Aomori 036-8564, Japan; [2]Department of Bioscience and Laboratory Medicine, Hirosaki University Graduate School of Health Sciences, Hirosaki, Aomori 036-8564, Japan; [3]Research Center for Biomedical Sciences, Hirosaki University, Hirosaki, Aomori 036-8564, Japan

Received January 28, 2025; Accepted July 14, 2025

DOI: 10.3892/mmr.2025.13645

**Abstract.** Patients with acute myeloid leukemia (AML) generally receive total body irradiation at a high-dose rate for the ablation of bone marrow cells, including AML cells. However, in rare cases, radioresistant AML cells appear, interfering with the therapeutic effect. HL60 cells were used to model a radioresistant leukemia cell line that emerged from repeated radiation exposure (Res-HL60). Notably, the mechanism through which microRNA (miRNA/miR) expression influences radioresistance in this model is unclear. In the current study, the expression profile of the miRNAs included in the small RNAs in Res-HL60 was analyzed using an miRNA microarray. A total of 1,187 miRNAs were retained for analysis after normalization. Among them, 27 miRNAs (10 upregulated and 17 downregulated in Res-HL60 cells compared with wild-type-HL60 cells) exhibited $P<0.05$ and fold change >1.5 or <0.66. Furthermore, the expression levels of five miRNAs were validated by reverse transcription-quantitative PCR: miR-146a-5p (upregulated), and miR-30c-1-3p, miR-671-5p, miR-610 and miR-3675-5p (downregulated). To investigate the target mRNAs of these five miRNAs, OmicsNet (ver. 2.0) was used. A total of 27 mRNAs were identified as targets of these multiple miRNAs. Furthermore, Reactome analysis revealed enrichment in the following processes 'Cell cycle, Mitotic' (R-HAS-69278), 'Apoptosis' (R-HAS-109581) and 'Immune system' (R-HAS-168256), suggesting that these miRNAs regulate genes involved in these pathways. These findings indicated that the altered expression of five specific microRNAs in radioresistant AML cells may be associated with radioresistant conditions through the modulation of mRNA expression.

*Correspondence to:* Professor Satoru Monzen, Department of Radiation Science, Hirosaki University Graduate School of Health Sciences, 66-1 Hon-cho, Hirosaki, Aomori 036-8564, Japan
E-mail: monzens@hirosaki-u.ac.jp

*Key words:* leukemia, radioresistant, HL60, microRNA, DNA fragments, bioinformatics

## Introduction

Leukemia disrupts the homeostasis of the hematopoietic system and causes abnormal proliferation of blast cells (1). Acute myeloid leukemia (AML), including its M2 subtype, reduces survival in adults; therefore, establishing effective treatment strategies is critical for improving prognosis (2,3). Chemotherapy, such as the '7+3' regimen, remains the standard first-line treatment for AML. However, in some relapsed or refractory cases, total body irradiation (TBI) is used as part of conditioning regimens before hematopoietic stem cell transplantation to eradicate residual leukemic cells (4,5). Repeated exposure to radiation in such settings may, in rare cases, contribute to the emergence of leukemic cells with reduced radiosensitivity, potentially impeding complete remission. Although the concept of 'radiation-resistant AML' is not widely recognized in clinical settings, where resistance is more commonly associated with chemotherapy, TBI has been implicated as a contributing factor in therapy-related AML (6). Furthermore, a phase II clinical trial evaluating treosulfan, fludarabine, and low-dose TBI in pediatric and young adult AML/MDS patients highlighted the clinical relevance and complex outcomes of TBI-based regimens, including relapse and non-relapse mortality (7). While radiation resistance is not a routine concern in AML treatment, these findings support the relevance of exploring the molecular basis of radiation response.

In the present study, we employed an *in vitro* AML model to investigate the acquisition of radioresistance. Specifically, we previously established a radioresistant AML cell line (Res-HL60) derived from HL60 cells, an AML M2 subtype cell line of human origin, and investigated the molecular mechanisms underlying radioresistance. Through repeated irradiation, the Res-HL60 cells acquired smaller morphology, increased proliferative potency, and showed elevated expression of CD38 cell surface antigen and several mRNAs (8-12). However, the upstream regulatory mechanism governing these gene expression changes remains unclear, necessitating further investigation.

MicroRNAs (miRNAs), a class of noncoding RNAs that regulate mRNA translation, have been implicated in cancer

progression and cell behavior, and their expression patterns are increasingly recognized as diagnostic and prognostic biomarkers (13,14). Additionally, miRNAs have emerged as potential therapeutic targets in cancer. Despite this, the profile of miRNA expression in radioresistant AML cells such as Res-HL60 has not been previously reported. Given that chromosomal abnormalities, epigenetic dysregulation, and impaired miRNA biogenesis, potentially triggered by frequent radiation exposure, can all influence miRNA expression (15), investigating these changes may help clarify the molecular basis of acquired radioresistance. Therefore, in this study, we performed transcriptome analysis focusing on miRNA expression in Res-HL60 cells to explore mechanisms associated with radioresistance in AML.

## Materials and methods

*Leukemia cell line and culture*. The human AML cell line HL60 (wild-type: Wt-HL60) was obtained from the RIKEN BioResource Center. The Res-HL60 cell line was generated by exposing Wi-HL60 cells to 4-Gy irradiation per week for 4 weeks. Wt-HL60 and Res-HL60 cells were cultured in RPMI-1640 medium (Thermo-Fisher Scientific, Inc.) supplemented with 10% heat-inactivated fetal bovine serum (Japan Bioserum, Inc.) and 1% penicillin/streptomycin (Thermo-Fisher Scientific, Inc.) in a humidified atmosphere containing 5% $CO_2$ at 37˚C. In this study, the control group was defined as non-irradiated Wt-HL60 cells cultured under these standard conditions (5% $CO_2$ and 95% air). The characteristics of Res-HL60 cells, including higher proliferative capacity, smaller cell size and altered chemical reactivity, have been reported previously by our group (8-12). In the present study, a time-course analysis of morphological changes in Res-HL60 cells was conducted (Fig. 1). Cells were initially seeded at a density of $2x10^5$ cells/ml on Day-1. X-ray irradiation was performed on Day 0. On Day 2 (i.e., the third day after initial seeding), cells were passaged and reseeded at $2x10^5$ cells/ml. When the cell density remained below $2x10^5$ cells/ml, only medium replacement was performed. No additional supplements (e.g., non-essential amino acids, sodium pyruvate) were added. To calculate the cumulative total viable cell number including all passages, the following formula was used: Cumulative cell number (/ml)=A x $[(2x10^5) + B]/(2x10^5)$, where 'A' is the viable cell number (cells/ml) measured up to Day 2 (before passaging), and 'B' is the net increase in viable cell number (cells/ml) from Day 3 onward, relative to the reseeded density ($2x10^5$ cells/ml). B=0 for Days 0-2. This method allowed us to reflect the overall proliferation dynamics across reseeding and media replacement steps. The updated y-axis label in Fig. 2A and B reflects this definition. To confirm the identity and authenticity of the cell lines used in this study, short tandem repeat (STR) profiling was performed. The STR profiles of both Wt-HL60 and Res-HL60 showed a perfect match with the reference profile for HL60 (Cellosaurus ID: CVCL_0002, URL: https://www.cellosaurus.org/CVCL_0002), as provided by the RIKEN BioResource Center, indicating no evidence of contamination or misidentification. The STR profiles are provided in Fig. S1 and Table SI.

*Irradiation*. X-ray irradiation (150 kVp, 20 mA with 0.5-mm aluminum and 0.3-mm copper filters) was performed using an X-ray generator (MBR-1520R-3; Hitachi Medical Co., Ltd.) at a distance of 45 cm between the focus and target. The dose was monitored during irradiation using a thimble ionization chamber set next to the sample. The dose rate was 1 Gy/min. The cultured cells were exposed to X-rays as previously described (8-12).

*Flow cytometry analysis*. Flow cytometry was performed using Cell Lab Quanta™ Sc MPL system (Beckman Colter Immunotech) to assess cell size, granularity, and CD38 surface expression. Unlike conventional flow cytometers that use forward scatter to estimate cell size, the Cell Lab Quanta utilizes Electric Volume (EV), which is based on the Coulter principle, to directly measure cell size via changes in electrical resistance as cells pass through an aperture. This method allows for accurate assessment of cell volume independent of optical scattering. Granularity, representing internal cellular complexity, was evaluated based on side scatter (SSC) intensity, as is standard in flow cytometry. CD38 expression was also assessed due to its dual relevance as both a hematopoietic differentiation marker and a potential indicator of acquired radioresistance. CD38 is a well-characterized surface antigen known to be markedly upregulated during granulocytic differentiation of HL60 cells (16). Furthermore, our previous studies demonstrated sustained CD38 expression in Res-HL60 cells even in the absence of differentiation-inducing agents, suggesting a role in the radioresistant phenotype (8-12). Based on these findings, CD38 was utilized in this study both as a marker of differentiation and as a surrogate indicator of radiation resistance.

*DNA fragmentation*. The Comet Assay Single Cell Gel Electrophoresis Assay (cat. no. 4250-050-K; TREVIGEN, Inc., Gaithersburg, USA) was used to evaluate the DNA fragments of the cells irradiated with X-rays. One day after seeding in a 60-mmφ culture dish at a concentration of $1.0x10^5$ cells/ml, the cells were irradiated with 1-4 Gy of X-rays, and the cells were collected after 24 h. The collected cells were fixed on glass slide (Matsunami Grass Inc., Osaka, Japan) using LM Agarose (TREVIGEN Inc.). The glass slide to which the sample was attached was immersed in an alkaline solution [200-mM NaOH, 1-mM ethylenediaminetetraacetic acid (EDTA)], and electrophoresis (21 V, 3 A, 30 min, 4˚C) was performed. After washing the glass slide with distilled water and 70% EtOH and drying, it was stained with 100 $\mu$l of a staining solution containing a mixture of SYBR Green (TREVIGEN Inc.) and TE Buffer (10-mM Tris, 1-mM EDTA). After drying, the tail moment was observed using a fluorescence microscope (OLYMPUS Inc.). Images were taken using Comet Assay IV (Instem, Conshohocken, USA) for observation purposes. Tail moment was calculated using the formula: Tail Moment=Tail Length x % Tail DNA/100, using Comet Assay IV software. This calculation reflects both the extent and the intensity of DNA fragmentation in individual cells.

*Extraction of total RNAs from cells*. Total intracellular RNAs (four replicates performed in parallel) were extracted using ISOGEN II (Nippon Gene Co., Ltd.) according to the

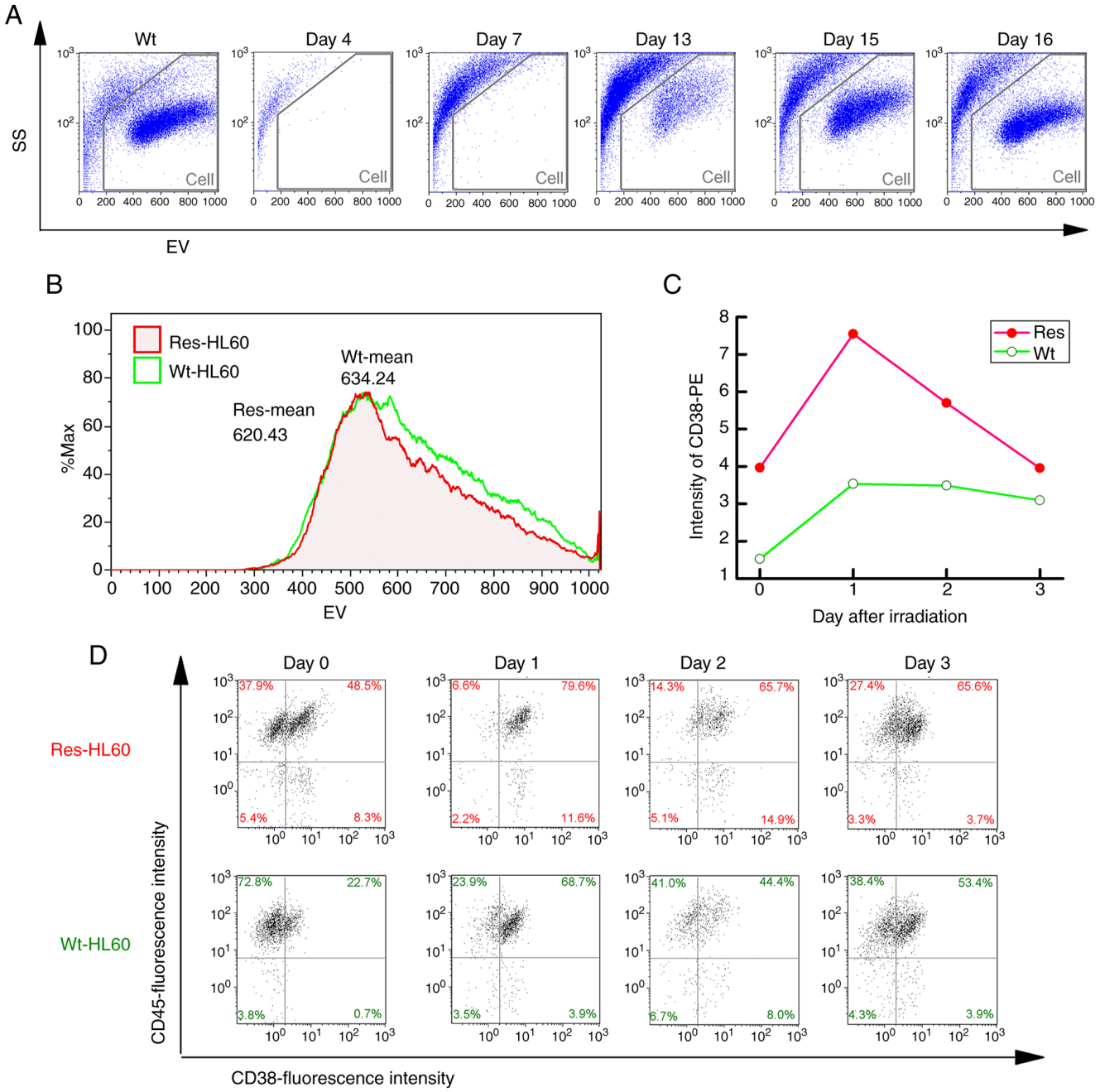


Figure 1. Characterization of Res-HL60 cell. (A) Cellular morphology and subpopulation characteristics were analyzed using flow cytometry. The horizontal and lateral axis indicate the mean size of the cell (EV) and the intracellular complexity (SS), respectively. (B) The EV histogram of each type of cell. (C) The time course of the CD38 expression intensity and (D) dot plots on the CD38-CD45 cell surface antigen after the exposure of 4-Gy X-ray is shown. Non-irradiated HL60 cells cultured under standard normoxic conditions (5% $CO_2$ and 95% air) were used as the control group in all analyses. Wt, wild type; Res, resistant; EV, electronic volume; SS, side scatter.

manufacturer's instructions. The purity and concentration of extracellular RNAs were assessed using a NanoDrop spectrophotometer (NanoDrop Technologies; Thermo-Fisher Scientific, Inc.). The RNA samples had 260/280-nm absorbance ratios of 1.8-2.0. Furthermore, the peaks of the small RNAs were confirmed using an Agilent 2100 Bioanalyzer (Agilent Technologies, Inc.).

*Microarray analysis of miRNAs*. SurePrint G3 human miRNA 8x60-K Microarray (Agilent Technologies Inc.) was used to analyze intracellular microRNA expression. Cyanine 3 labeling was performed with 1 ng of intracellular microRNA using an miRNA Complete Labeling and Hybridization kit (Agilent Technologies Inc.), following the manufacturer's instructions. After hybridization and washing of the microarray slide, fluorescence image scanning was performed using a SureScan G 2600 D (Agilent Technologies Inc.). The expression data were processed using GeneSpring GX14.5 (Agilent Technologies, Inc.) to normalize the quantiles of all values in the respective microarrays. The obtained microarray data were registered with the Gene Expression Omnibus (GEO) (GSE285934).

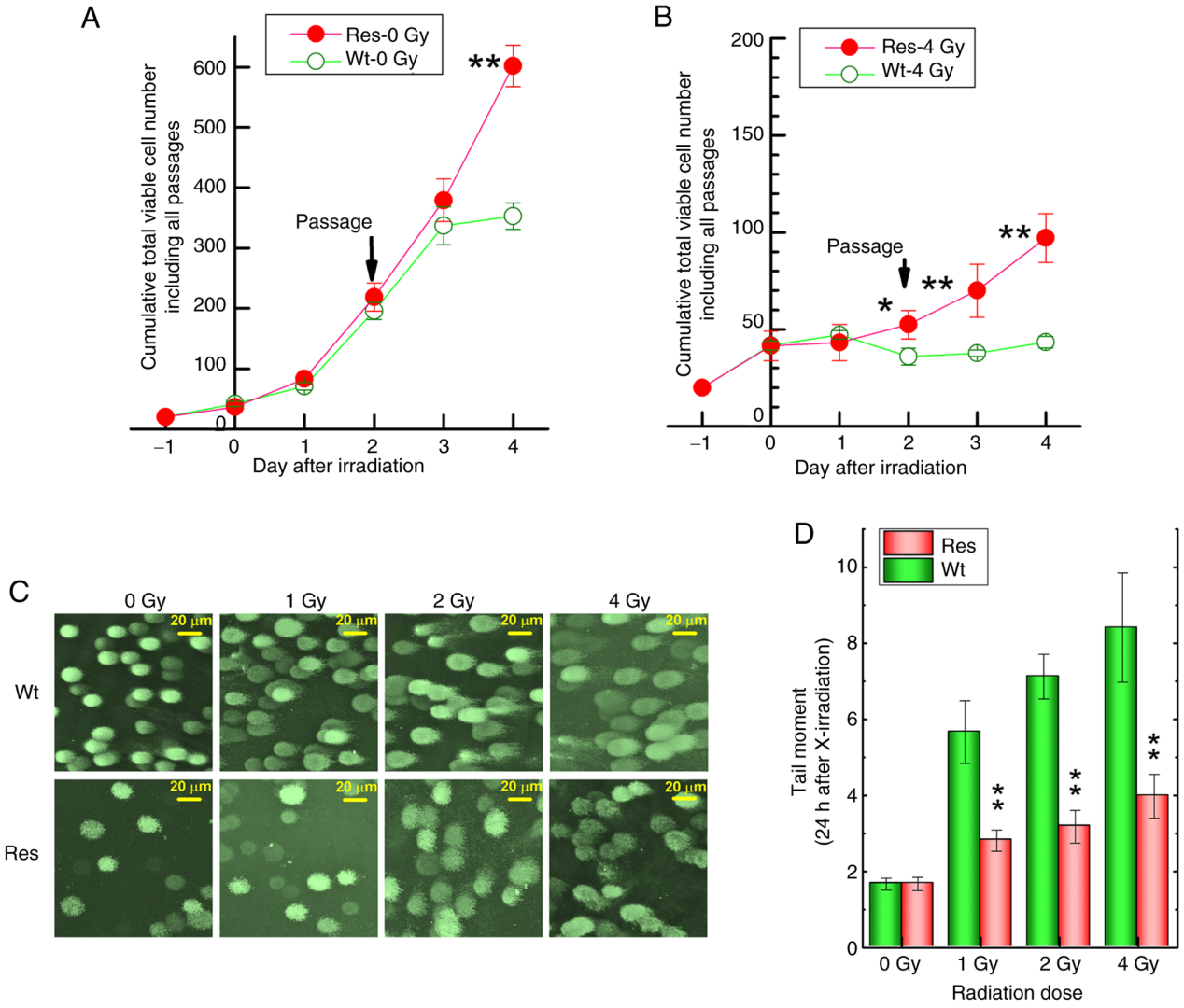


Figure 2. Cell proliferation curve and DNA fragmentation analysis. (A) Cumulative proliferation of Wt-HL60 and Res-HL60 cells under non-irradiated conditions. Cells were seeded at $2x10^5$ cells/ml on Day-1 and cultured without irradiation. On Day 2, the cells were passaged to maintain the same seeding density. If cell density remained below this threshold, only the medium was replaced without passaging. The cumulative number of viable cells was calculated using the formula: Cumulative cell number (/ml)=A x [$(2x10^5)$ + B]/$(2x10^5)$, where 'A' is the viable cell number up to Day 2, and 'B' is the net increase from Day 3 onward relative to the reseeding density. (B) Cumulative proliferation of Wt-HL60 and Res-HL60 cells under 4-Gy irradiated conditions. The same seeding and passaging protocol as in (A) was followed, except that the cells were exposed to 4 Gy of X-ray irradiation on Day 0. Cell proliferation was then monitored to assess the impact of irradiation on the growth of wild-type and resistant HL60 cells. Cumulative viable cell numbers were calculated using the same formula as in (A). (C) Representative images of the comet assay showing DNA damage 24 h after X-ray exposure at doses of 1-4 Gy. (D) Quantification of DNA damage based on tail moment calculated from the comet assay shown in (C). Data are shown as the mean ± standard error of the mean from four independent experiments. $^*$P<0.05, $^{**}$P<0.01 vs. Wt-HL60, determined by unpaired Student's t-test. Wt, wild type; Res, resistant.

*Reverse transcription-quantitative PCR (RT-qPCR) analysis.* First-strand cDNA was synthesized using Mir-X™ miRNA First-Strand Synthesis Kit (Takara Bio Inc., Otsu, Japan; Cat. Nos. 638313) according to the manufacturer's protocol (Protocol No. PT5001-1). MiRNA expression was assessed by qPCR using TB Green Advantage qPCR Premix (Takara Bio Inc., Cat. Nos. 639676) on a SmartCycler® II system (Takara Bio Inc.). The thermocycling conditions were as follows: 95˚C for 10 sec, followed by 40 cycles of 95˚C for 5 sec and 60˚C for 20 sec. Relative miRNA expression levels were calculated using the $2^{-\Delta\Delta Cq}$ method. U6 small nuclear RNA, included as an internal control primer set in the Mir-X™ First-Strand Synthesis Kit (Takara Bio Inc., Cat. Nos. 638313), was used for normalization. The exact primer sequences for U6 were not publicly disclosed, and direct inquiries to the manufacturer did not yield this information. However, the Mir-X™ system is widely used and has been independently validated in numerous peer-reviewed studies for reliable miRNA quantification. We adhered strictly to the manufacturer's standardized protocol to ensure data reproducibility and accuracy. For the analysis ΔCq was calculated as (Cq of target miRNA-Cq of U6). ΔΔCq was defined as (ΔCq of Res-HL60-ΔCq of Wt-HL60), and fold change was calculated as $2^{-\Delta\Delta Cq}$, with Wt-HL60 set as the baseline (fold change-1) (17). Sequences of the target miRNAs were obtained from the miRBase database (https://www.mirbase.org/). MiRNA-specific forward primers were synthesized by Eurofins Genomics Inc. and are listed in Table I. A universal reverse primer provided in the Mir-X™ kit was used for all miRNAs. The Mir-X™ qRT-PCR system employs a poly(A)-tailing strategy followed by reverse transcription

Table I. Sequences of miRNA primers for reverse transcription-quantitative PCR.

| Primer name | Accession no. | Sequence, 5'-3' |
|---|---|---|
| hsa-miR-3612 | MIMAT0017989 | AGGAGGCATCTTGAGAAATGGA |
| hsa-miR-324-5p | MIMAT0000761 | CGCATCCCCTAGGGCATTGGTG |
| hsa-miR-146a-5p | MIMAT0000449 | TGAGAACTGAATTCCATGGGTT |
| hsa-miR-1246 | MIMAT0005898 | AATGGATTTTTGGAGCAGG |
| hsa-miR-3190-3p | MIMAT0022839 | TGTGGAAGGTAGACGGCCAGAGA |
| hsa-miR-3156-5p | MIMAT0015030 | AAAGATCTGGAAGTGGGAGACA |
| hsa-miR-124-3p | MIMAT0000422 | TAAGGCACGCGGTGAATGCCAA |
| hsa-miR-9-3p | MIMAT0000442 | ATAAAGCTAGATAACCGAAAGT |
| hsa-miR-324-3p | MIMAT0000762 | CCCACTGCCCCAGGTGCTGCTGG |
| hsa-let-7e-5p | MIMAT0000066 | TGAGGTAGGAGGTTGTATAGTT |
| hsa-miR-3669 | MIMAT0018092 | TACGGAATATGTATACGGAATAT |
| hsa-miR-29b-3p | MIMAT0000100 | TAGCACCATTTGAAATCAGTGTT |
| hsa-miR-30c-1-3p | MIMAT0004674 | CTGGGAGAGGGTTGTTTACTCC |
| hsa-miR-671-5p | MIMAT0003880 | AGGAAGCCCTGGAGGGGCTGGAG |
| hsa-miR-425-5p | MIMAT0003393 | AATGACACGATCACTCCCGTTGA |
| hsa-miR-345-5p | MIMAT0000772 | GCTGACTCCTAGTCCAGGGCTC |
| hsa-miR-610 | MIMAT0003278 | TGAGCTAAATGTGTGCTGGGA |
| hsa-miR-4260 | MIMAT0016881 | CTTGGGGCATGGAGTCCCA |
| hsa-miR-376c-3p | MIMAT0000720 | AACATAGAGGAAATTCCACGT |
| hsa-miR-512-3p | MIMAT0002823 | AAGTGCTGTCATAGCTGAGGTC |
| hsa-miR-744-3p | MIMAT0004946 | CTGTTGCCACTAACCTCAACCT |
| hsa-miR-27b-3p | MIMAT0000419 | TTCACAGTGGCTAAGTTCTGC |
| hsa-miR-7-2-3p | MIMAT0004554 | CAACAAATCCCAGTCTACCTAA |
| hsa-miR-769-3p | MIMAT0003887 | CTGGGATCTCCGGGGTCTTGGTT |
| hsa-miR-3675-5p | MIMAT0018098 | TATGGGGCTTCTGTAGAGATTTC |
| hsa-miR-101-5p | MIMAT0004513 | CAGTTATCACAGTGCTGATGCT |
| hsa-miR-20b-5p | MIMAT0001413 | CAAAGTGCTCATAGTGCAGGTAG |

miR, microRNA.

with an adapter-anchored oligo(dT) primer. This approach selectively amplifies mature polyadenylated miRNAs, while excluding pre-miRNAs, long non-coding RNAs, and host transcripts lacking poly(A) tails. The specificity of the amplification was further supported by the observation of single, sharp melt curve peaks in all reactions.

*Statistical analysis*. Statistical analyses were performed using the Origin software package (Pro version 9.0; OriginLab Corporation, Northampton, MA, USA) and Microsoft Excel (Microsoft Office 365). To evaluate the statistical significance of differences between the control and experimental groups, an unpaired Student's t-test was used, as the data met assumptions for parametric testing. All results are presented as the mean ± SEM based on four independent experiments. $P<0.05$ was considered to indicate a statistically significant difference.

## Results

*Analysis of cell damage exposed to IR*. The cell population exposed to 4-Gy radiation temporarily disappeared but reappeared on days 15-16 (Fig. 1A). However, it was confirmed that Res-HL60 had a decreased EV (Wt: 634.24, Res: 620.43) (Fig. 1B). Furthermore, the expression of the CD38 cell surface antigen in Res-HL60 cells was significantly increased after radiation compared with that in the wild-type cells (maximum on day 1: Res=7.55±0.53, Wt=3.54±0.89), confirming a similar previously reported response (Fig. 1C and D). In our previous study, we evaluated CD38 as a differentiation marker and found that its expression was consistently elevated in Res-HL60 cells (8). The Res-HL60 cells seeded at $1x10^5$ cells/ml exhibited approximately 30-fold proliferation ($3.1±0.4x10^5$ cells/ml) on day 5, and the Wt-HL60 cells exhibited approximately 15-fold proliferation ($1.6±0.1x10^5$ cells/ml) (Fig. 2A). The 4-Gy irradiation condition of Res-HL60 cells was also maintained approximately 5-fold after exposure on day 4 ($4.9±0.5x10^5$ cells/ml); however, it remained at the level observed on day 0 in Wt-HL60 cells ($1.9±0.1x10^5$ cells/ml) (Fig. 2B). The extent of DNA damage caused by radiation exposure in these cells was determined using a comet assay (Fig. 2C). The tail moment of Res-HL60 cells irradiated with 1-4 Gy was similar to that observed in cells without irradiation, whereas the tail moment of Wt-HL60 cells exposed to irradiation was significantly increased (Fig. 2D).

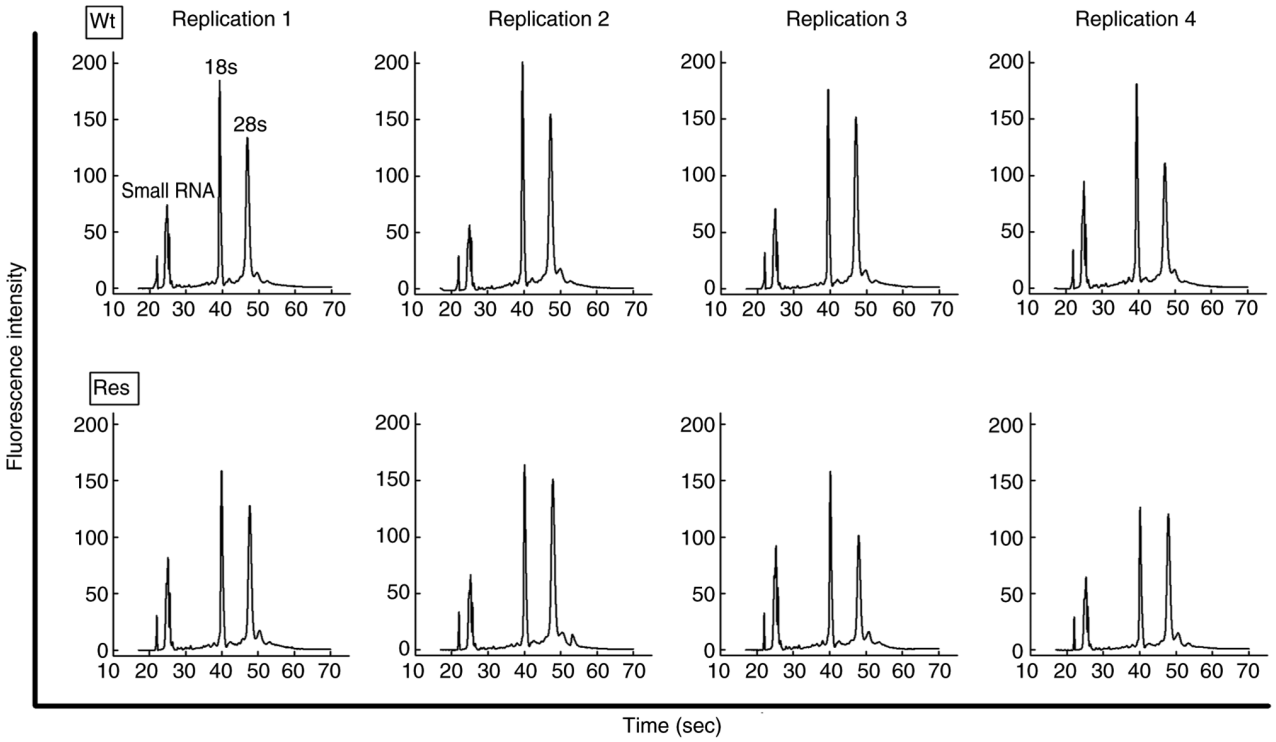


Figure 3. Histogram of total RNA detection from Res-HL60 and Wt-HL60 cells. Total RNA was detected in each cell using an Agilent 2100 bioanalyzer. Wt, wild type; Res, resistant.

*Expression profiles of miRs*. To clarify the miRNA expression profiles of Res-HL60 cells, total RNAs were extracted from these cells. Using an Agilent bioanalyzer, the extracted total RNAs were confirmed to have an RIN value (max-10) and rRNA 18s and 28s peaks, which reveal whether small RNAs, including miRNAs, are of sufficient concentration and quality for analysis (Fig. 3). Total RNAs extracted from each cell exhibited an RIN >9 in all samples. Furthermore, the peak of small RNAs, 18s, and 28s in the histogram was cleared, and these samples were considered to have good quality for RNA analysis (Table II).

After miRNA microarray analysis, data were extracted after quantile normalization, excluding under background, and collection of unsaturated signals (Fig. 4A). After processing, the signal values obtained using multiple types of detection probes were averaged for each miRNA name, yielding 1,187 miRNA data. Among the miRNAs that significantly increased or decreased in Res compared with Wt, 10 miRNAs had a fold change (Res/Wt) >1.5, and 17 miRNAs had a fold change (Res/Wt) <0.66 (Fig. 4B-D). For the 27 miRNAs that exhibited expression changes in the microarray analysis, a functional enrichment analysis using the Reactome Pathway Database in OmicsNet 2.0 was performed to estimate the associated mRNA expression pathways. Cellular functional changes were observed in the following pathways: 'Immune System (R-HAS-168256)', 'Signaling by PGDF (R-HAS-186797)', 'Adaptive Immune System (R-HAS-1280218)', 'Signaling by EGFR in Cancer (R-HAS-1643713)', 'Apoptosis (R-HAS-109581)', and 'Cell Cycle, Mitotic (R-HAS-69278)' for tumor growth and/or invasion (Fig. 5A).

Furthermore, when we focused on the functional analysis of the target mRNAs of the 10 upregulated miRNAs in Res-HL60 cells, these mRNAs were strongly related to the following functional pathways: 'cell cycle', 'cell division' and 'apoptosis' (Fig. 5B). In contrast, the target mRNAs of the 16 downregulated miRNAs in Res-HL60 cells were strongly related to the following functional pathways: 'Signaling by PDGF' and 'Assembly of collagen fibrils and other multimeric structures (R-HAS-2022090)' (Fig. 5C).

*Validation of the expression of 27 miRNAs*. The significant expression of the 27 miRNAs obtained from these microarray analysis signals was reconfirmed by RT-qPCR. Thus, the expression of miRNA-146a-5p was significantly increased, whereas the expression of miRNA-30c-1-3p, miRNA-671-5p, miRNA-610, and miRNA-3675-5p was significantly decreased (Fig. 6).

*Analysis of bioinformatics:* The mRNA networks controlled by the five reproduced miRNAs were analyzed using OmicsNet 2.0. In this network, 28 mRNAs were associated with two or more miRNAs (Fig. 7). Of these 28 target mRNAs, seven (i.e., ALG10B, CCDC6, CCND2, CPM, CYBRD1, NACC1, and UMPS) were targeted by miRNA-146a-5p, which is an upregulated miRNA, and the other four miRNAs, which are downregulated. Furthermore, three miRNAs (i.e., miRNA-610, miRNA-671-5p, and miRNA-30c-1-3p) targeted superoxide dismutase 2 (SOD2). In the Target Scan analysis, three miRNAs (miRNA-610, miRNA-671-5p, and miRNA-30c-1-3p) were predicted to bind to the 3'-UTR region of SOD2, which was predicted as the target mRNA (Fig. 8). Furthermore, two miRNAs (i.e., miRNA-671-5p and miRNA-30c-1-3p) were predicted to bind to the 3'-UTR region of MYH9 mRNA. The putative target sites of miR-610 and miR-30c-1-3p for CD38

Table II. Concentration and quality of total RNA extracted from Res-HL60 cells and Wt-HL60 cells.

| Sample list | Concentration of total RNA, $\mu$g/$10^6$ cells | RNA integrity number | Ratio of rRNA, 28s/18s |
|---|---|---|---|
| Wt | | | |
| Replication 1 | 3.6 | 9.5 | 1.03 |
| Replication 2 | 5.6 | 9.5 | 0.98 |
| Replication 3 | 6.5 | 9.6 | 1.16 |
| Replication 4 | 4.4 | 9.1 | 0.84 |
| Mean ± SE | 5.0±0.6 | 9.4±0.1 | 1.0±0.1 |
| Res | | | |
| Repliction 1 | 5.5 | 9.4 | 0.98 |
| Replication 2 | 4.3 | 9.6 | 1.18 |
| Replication 3 | 3.6 | 9.2 | 0.76 |
| Replication 4 | 4.1 | 9.6 | 1.13 |
| Mean ± SE | 4.4±0.3 | 9.5±0.1 | 1.0±0.1 |

rRNA, ribosomal RNA; Wt, wild type; Res, resistant; SE, standard error.

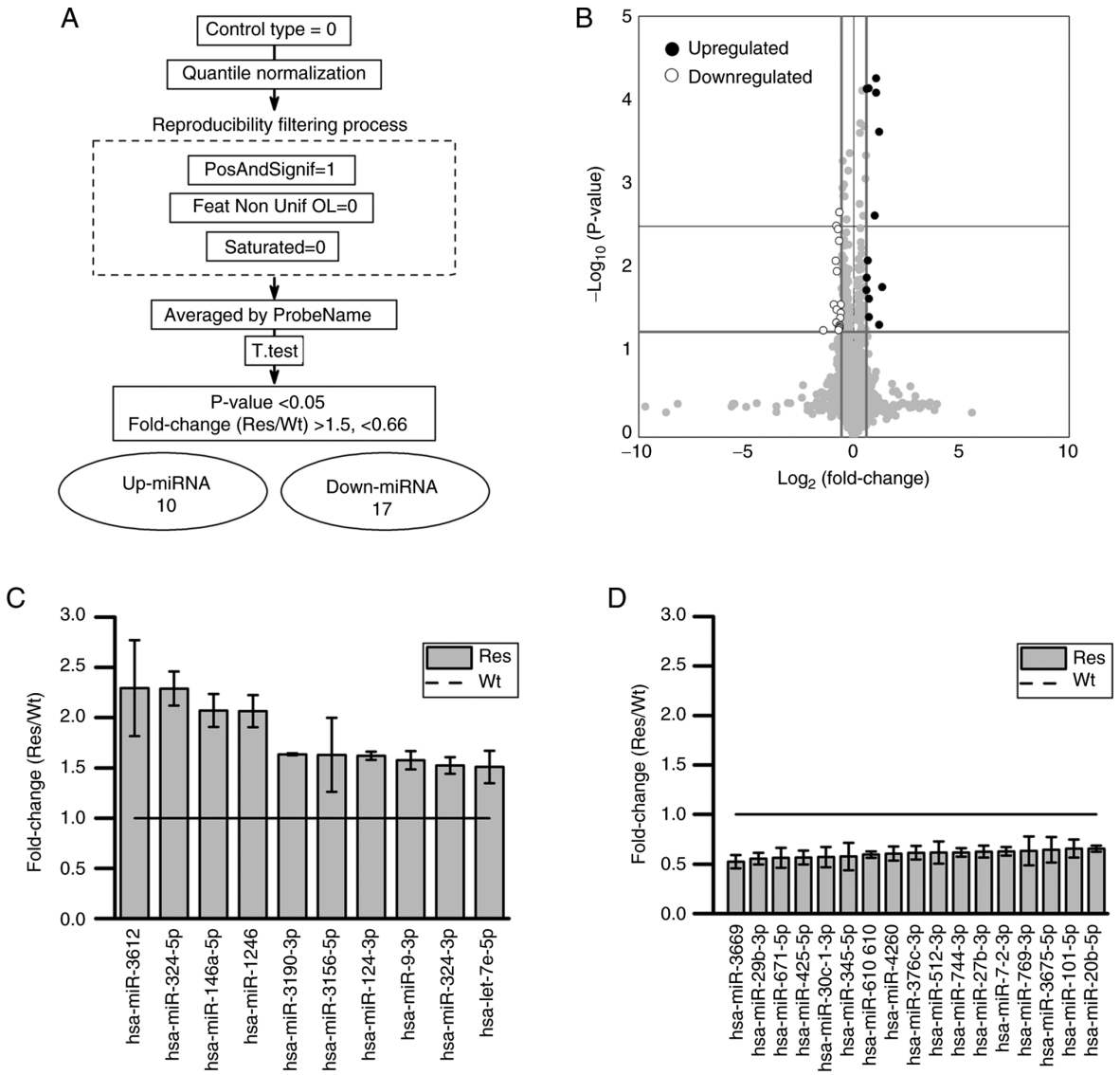


Figure 4. miRNA microarray analysis. (A) Statistical analysis for normalization, and the (B) relationship between fold change and P-value. (C) Significant upregulated miRNAs (P<0.05 by Student's t-test, >1.5 fold change), and (D) significant downregulated miRNAs (P<0.05 by Student's t-test, <0.66 fold change). The data are presented as the mean ± standard error of the mean of four experiments. miRNA/miR, microRNA; Wt, wild type; Res, resistant.

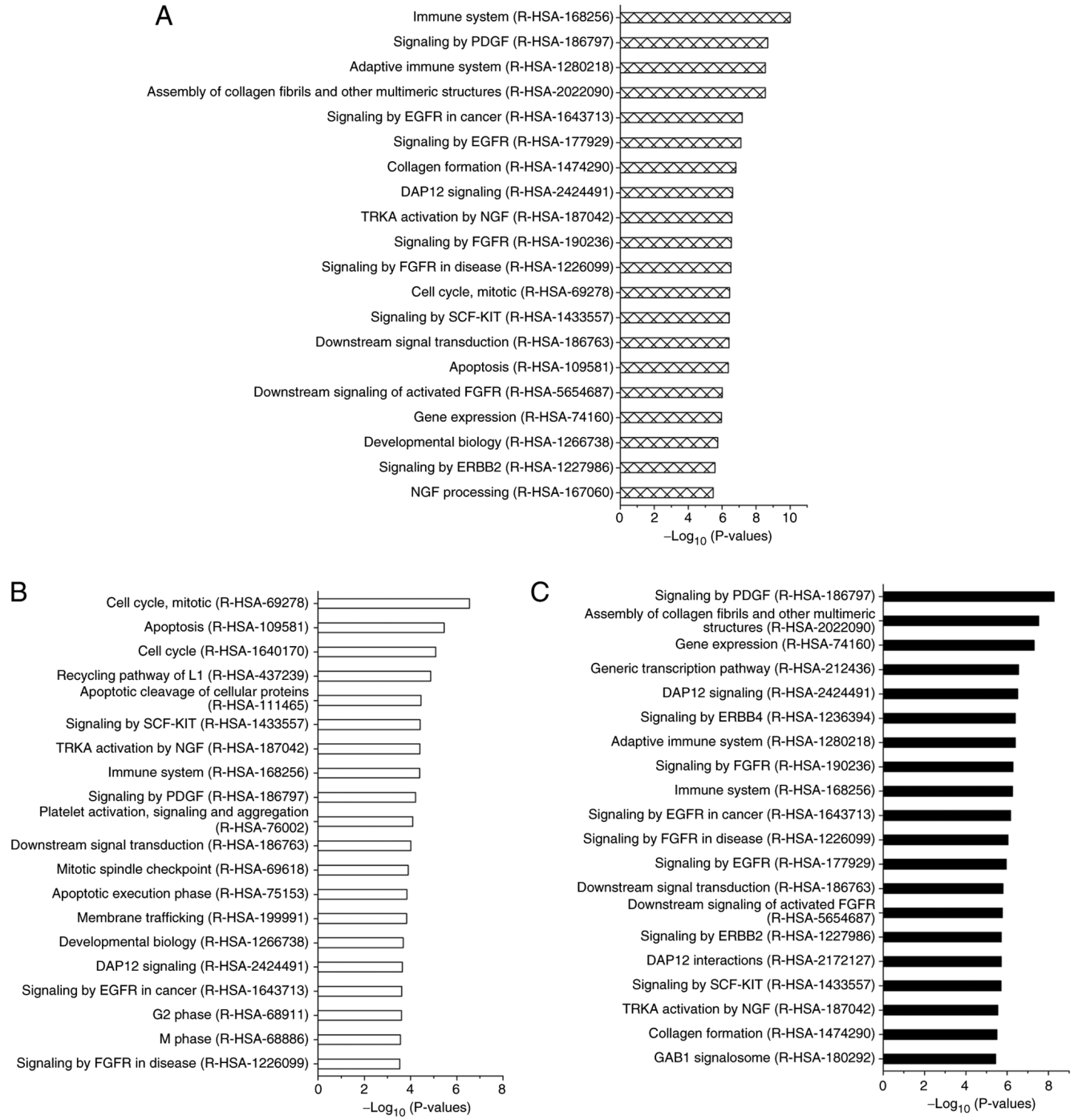


Figure 5. Top 20 enriched Reactome pathways associated with predicted target genes of differentially expressed miRNAs. Pathway enrichment analysis was conducted using the Reactome Pathway Database to categorize the predicted target genes of significantly altered miRNAs into curated biological pathways. Reactome pathway identifiers are shown in parentheses. Bar graphs show the top 20 enriched pathways ranked by statistical significance for the predicted target genes of (A) all 27 differentially expressed miRNAs, (B) 10 upregulated miRNAs and (C) 17 downregulated miRNAs. miRNA, microRNA.

mRNA and miR-3675-5p, miR-671-5p, and miR-30c-1-3p for ATM mRNA were located in the 3'-UTR region.

## Discussion

In this study, we analyzed the miRNA expression profile of a radioresistant AML cell model (Res-HL60) derived from the HL60 cell line, which belongs to the FAB M2 subtype of AML. We reconfirmed that Res-HL60 cells, which were established by repeated irradiation of HL60 cells, maintained the morphological characteristics previously described, even when remade (Fig. 1). The HL60 cell line, which is derived from a patient with AML, exhibits inherently low CD38 expression, as previously reported (18). We have previously evaluated CD38 as a differentiation marker and found that its expression was consistently elevated in Res-HL60 cells (8). In this study, we observed transient increases in CD38 expression immediately after irradiation. This upregulation has been reported to be associated with cellular activation and proliferation (19). CD38 was selected as the primary marker in this

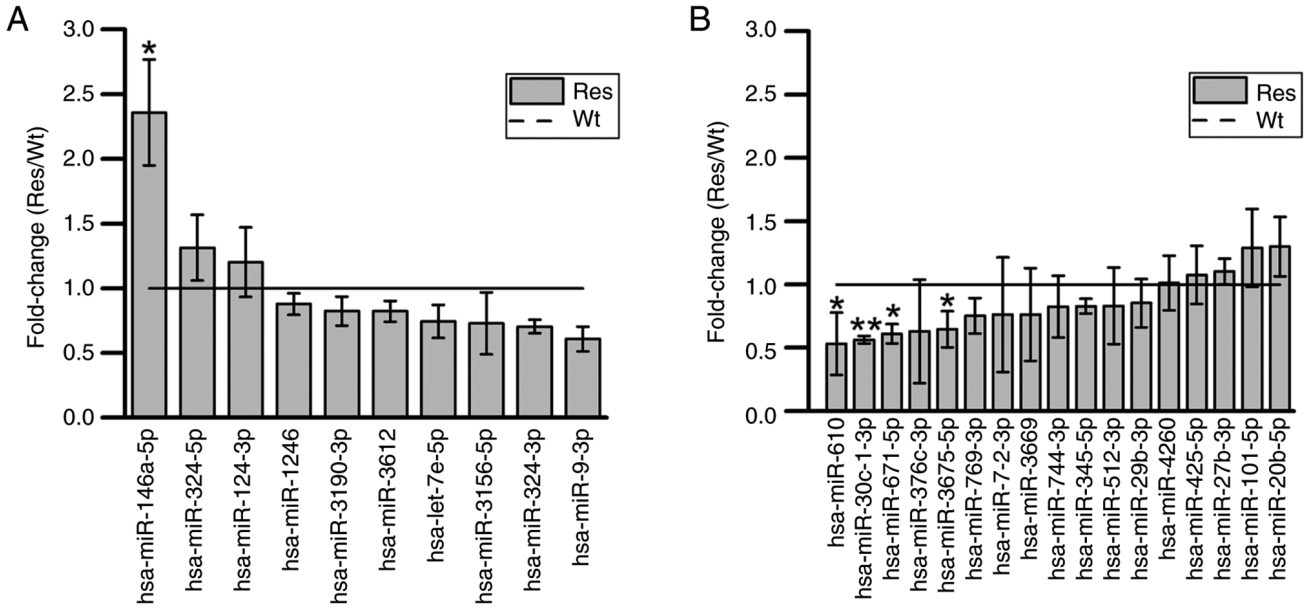


Figure 6. Validation analysis of the 27 focused miRNAs by RT-qPCR. (A) Upregulated miRNA and (B) downregulated miRNA group were validated by RT-qPCR. The quantitation by fluorescence signal was performed using the ΔΔCq method. U6 small nuclear RNA was used as the internal control. Fold change was calculated by comparing Res-HL60 cells to Wt-HL60 cells after normalization to U6 expression. Expression values in Wt-HL60 were set to 1, and fold change values in Res-HL60 are shown relative to this baseline (horizontal line). The data are presented as the mean ± standard error of the mean of four experiments. $^{**}$P<0.01, $^{*}$P<0.05 by unpaired Student's t-test. RT-qPCR, reverse transcription-quantitative PCR; miRNA/miR, microRNA; Wt, wild type; Res, resistant.

study because it is a well-established differentiation-associated antigen in the HL60 model system; its expression increases markedly during granulocytic differentiation, as demonstrated by Partida-Sánchez *et al* (16). In our Res-HL60 cells, CD38 consistently showed strong upregulation both under baseline conditions and immediately after irradiation. These observations, combined with CD38's known roles in $NAD^+$-dependent calcium signaling and immune modulation, made it a biologically relevant candidate for investigating radioresistant phenotypes in AML. Although Breitman *et al* broadly discussed the HL60 differentiation model, CD38-specific functional insights were established in later work (20). In this context, 'cellular activation' refers to an increased responsiveness of cells to external stimuli, such as radiation, typically accompanied by changes in surface markers, including CD38 upregulation. Although direct functional activation markers were not assessed in this study, similar CD38 upregulation has been correlated with cell activation and immune modulation in leukemia models. Our previously established Res-HL60 cells demonstrated enhanced proliferative capacity compared to Wt-HL60 cells, as evidenced by shortened population doubling times and increased viable cell counts (8-12). Although these proliferation characteristics were not re-evaluated in the present study, the phenotypic stability and CD38 expression patterns observed here are consistent with those findings.

Furthermore, DNA fragments did not increase in these cells due to radiation, and the response was confirmed to be similar to γ-H2AX, a marker for DNA double-strand breaks, and to previous DNA ladder analyses (9,21). In these damage responses in Res-HL60 cells, 27 miRNAs (10 upregulated and 17 downregulated) showed altered expression in the microarray analysis. Among them, five miRNAs (miR-146a-5p, miR-30c-1-3p, miR-671-5p, miR-610, and miR-3675-5p) consistently demonstrated significant changes in the same direction across both microarray and RT-qPCR validation experiments. This consistency suggests that these five miRNAs may play a regulatory role in modulating molecular pathways associated with the development of radiation resistance. These five miRNAs have been implicated in tumor proliferation, radiosensitivity, and hematopoiesis (22-30). miR-146a functions together with TRAF1 and IRAK1 as negative feedback factors for the two toll-like receptor pathway proteins (22). It is also involved in regulating the transcriptional activity of NF-κB, which is necessary for the differentiation of hematopoietic cells (23,24). In radiotherapy for meningioma, the expression of miR-30c-1-3p is suppressed when treatment resistance occurs (25). In another report, the suppression of miR-30c-1-3p expression was associated with the progression of prostate cancer (26). The overexpression of miR-671-5p has been shown to significantly increase apoptosis and DNA damage in human glioblastoma cells (27). In neuroblastoma cells, the overexpression of miR-610 induces apoptosis and reduces cell viability (28). miR-3651 promotes the proliferation of hepatocellular carcinoma and colorectal cancer cells (29,30). These reports from various cell types suggest that changes in miRNA expression in radioresistant AML are triggered by cell viability activity.

The analysis of linking target mRNA networks of five miRNAs with radioresistant AML is new information, and 11 target mRNAs of these miRs (i.e., ALG10B, CCDC6, CCND2, CPM, CYBRD1, NACC1, UMPS, SOD2, MYH9, CD38, and ATM) may regulate the expression of its associated proteins and transcription factors in a complex manner. SOD2 can scavenge active oxygen produced by radiation irradiation, and SOD2 has been reported to protect against cellular stress (31). Furthermore, MYH9 is involved in cell division, cell

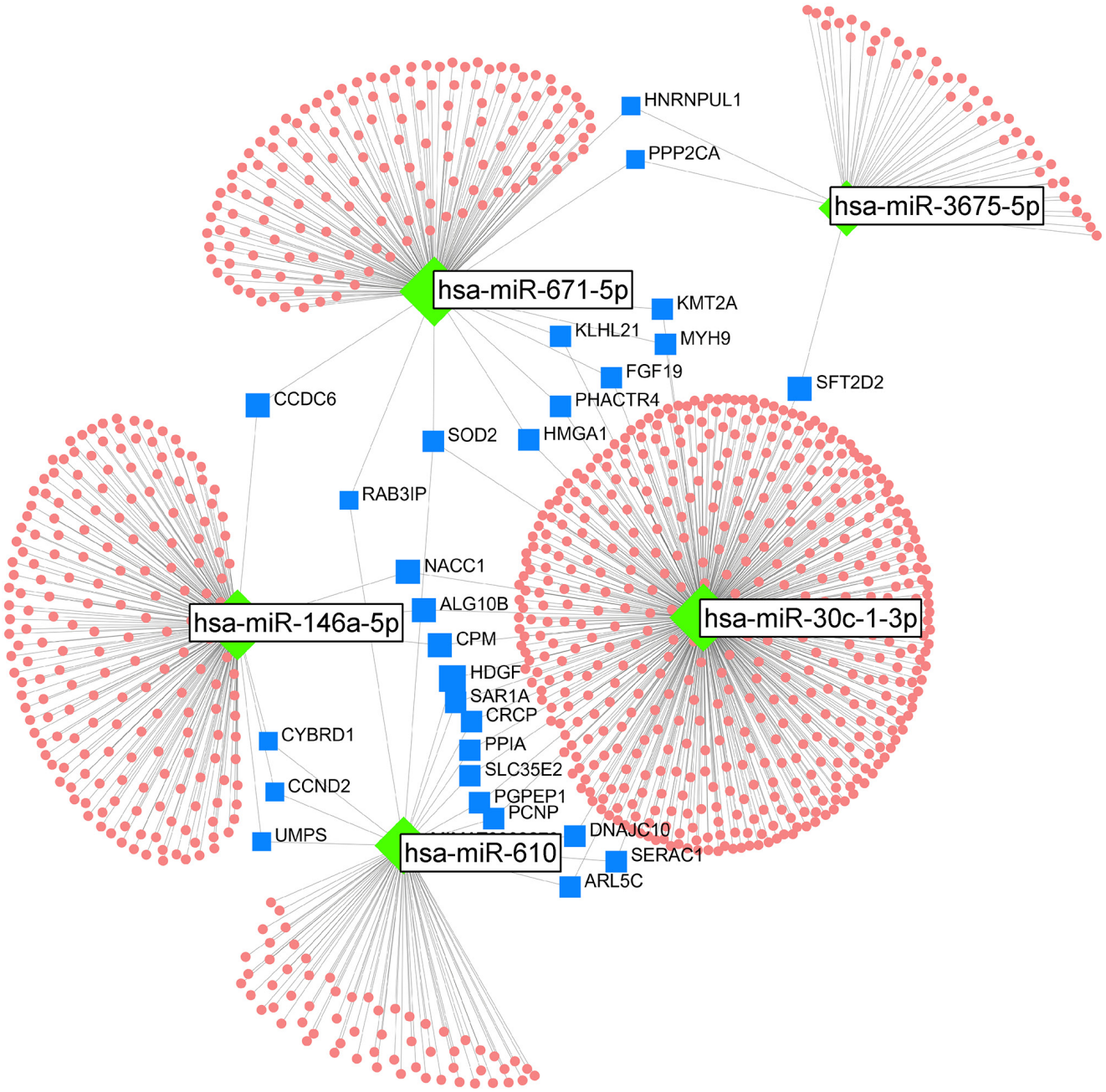


Figure 7. Predictive network analysis between miRNA and its target mRNA using OmicsNet. OmicsNet was used to predict the target genes. This study used the Reactome database of OmicsNet to predict the target genes. Lines connect the miRNA target genes. The figure shows green for miRNAs, blue for target genes, and red for other related genes. miRNA/miR, microRNA.

migration, and maintenance of cell morphology and acts as an antiapoptotic agent in head and neck cancers where MYH9 is highly expressed (32). Moreover, it also reduces intracellular reactive oxygen species levels through the activation of the MAPK signaling pathway and Nrf2/keap1 pathway and the promotion of the production of the antioxidant enzyme GCLC. It is also involved in radioresistance. This observation may also explain the morphological stability and resistance to radiation-induced apoptosis observed in Res-HL60 cells. To further investigate the clinical relevance of these target genes, we examined publicly available AML gene expression datasets from The Cancer Genome Atlas (TCGA) and the Gene Expression Omnibus (GEO). Yu *et al* have reported that MYH9 overexpression was significantly associated with poor prognosis in patients with AML based on TCGA-LAML data (33). This finding is also supported by GSE12417 (GEO), a dataset originally published by Metzeler *et al* (34), which includes cytogenetically normal AML cases. In a recent analysis by Zhai *et al* (35), MYH9 was among the genes linked to adverse outcomes in this cohort. Expression of ATM, although not frequently mutated in AML, has been implicated in treatment responses; low ATM expression enhances sensitivity to FLT3 inhibitors and may affect DNA damage signaling (36). SOD2 has not been directly studied in AML; however, it plays a key role in scavenging reactive oxygen species. A meta-analysis of pan-cancer TCGA datasets by Noh *et al* (31) reported that

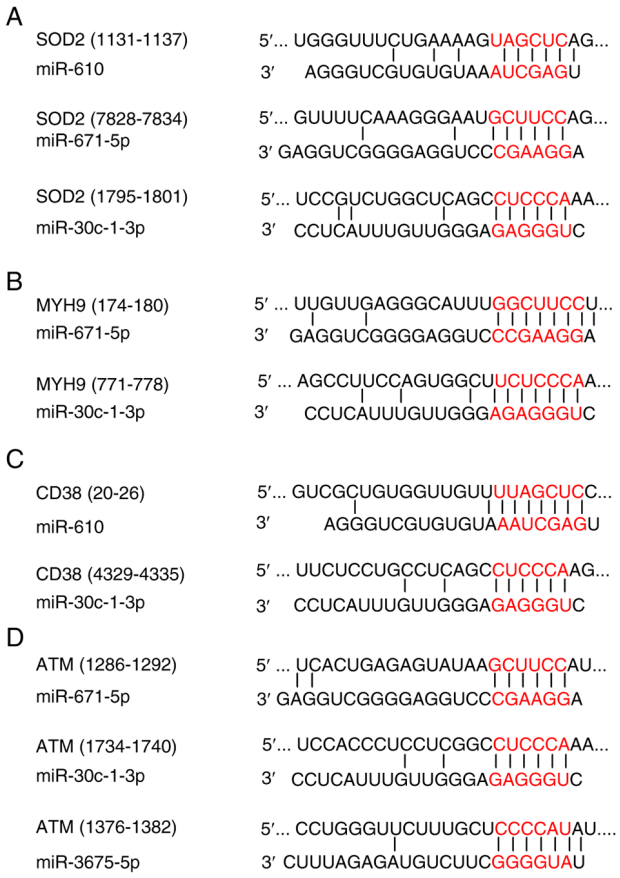


Figure 8. Target scan analysis in humans. The images show a predictive region for adhesion by target mRNA on 3'UTR and miRNA. The data show (A) SOD2, (B) MYH9, (C) CD38 and (D) ATM. miRNA/miR, microRNA; SOD2, superoxide dismutase 2.

SOD2 upregulation is associated with treatment resistance, suggesting its potential role in radioresistant phenotypes. We note that original survival analyses were not performed in this study. Instead, we relied on published results from previous analyses of these public datasets. This approach was taken due to the experimental focus of our study on the HL60-derived model. However, we fully acknowledge the importance of such analyses in increasing the translational relevance of our findings. While we agree with the reviewer's suggestion to perform updated survival analyses using the most recent TCGA and GEO datasets, this was beyond the scope of the current *in vitro* study. Nonetheless, incorporating such analyses is a clear objective for future work. We plan to conduct comprehensive bioinformatics evaluations of MYH9, ATM, and SOD2 expression in larger patient cohorts using integrated clinical and molecular data. Furthermore, the use of radiation-resistant AML patient samples to validate these gene targets was not feasible in the present study due to sample unavailability. However, this represents a crucial next step. Future studies will aim to collect and analyze patient-derived AML samples, particularly from individuals with known radiation treatment history, to directly confirm the relevance of MYH9, ATM, and SOD2 in clinical radioresistance. These findings complement our *in vitro* results and support the relevance of SOD2, ATM, and MYH9 in AML radioresistance.

Most functions inferred from the Reactome analysis were related to anti-apoptotic processes and were associated with upregulated miR-146a-5p. Our original hypothesis was that miR-146a-5p promotes apoptosis by inhibiting antiapoptotic molecules, thereby enhancing radiosensitivity in Res-HL60 cells. However, the results of the inhibition of anti-apoptotic molecules did not support this hypothesis. Instead, these findings suggest that miR-146a-5p regulates an alternative pathway that could contribute to radiation resistance. *Target-scan* analysis revealed that the high expression of CD38 cell surface antigen protein, CD38 mRNA, and intracellular ATM is related to the regulation of the five miRNAs revealed here (Fig. 8). These miRNA regulations provide molecular biology information supporting previous cellular responses. This information enhances our understanding of the molecular mechanisms underlying radiation resistance in AML. To further elucidate the mechanisms linking CD38 expression and radiation resistance, our future studies will focus on dissecting the intracellular signaling pathways downstream of CD38. Specifically, we plan to investigate $NAD^+$ metabolism and calcium signaling pathways, both of which are regulated by CD38 and are known to affect cell survival, DNA repair capacity, and oxidative stress responses. These pathways may provide crucial mechanistic links between CD38 expression and the observed radioresistant phenotype in AML cells. In addition, combining CD38 expression analysis with metabolic profiling may help clarify its functional relevance in therapeutic resistance. This approach may also reveal novel therapeutic targets to overcome resistance in CD38-expressing AML subtypes. Although CD38 was a useful marker in our initial evaluation, we recognized that other markers, such as CD34, CD123, and ALDH are also relevant in the context of leukemia stemness and therapy resistance. Exploring the role of these markers was not within the scope of this study. However, future studies incorporating a broader panel of surface markers are warranted to further elucidate the mechanisms of AML radioresistance.

One limitation of this study is the lack of a regulatory analysis for the expression of the five miRNAs in AML cells, including investigations of intracellular signaling pathways and knockdown of the 11 predicted target mRNAs. Another limitation is that all experiments were performed using a single cell line, HL60, and its derived radioresistant subline. Although HL60 is a widely used model for AML studies, it does not capture the full genetic and phenotypic heterogeneity of AML, which can significantly affect radiosensitivity and miRNA profiles. Therefore, caution should be exercised when generalizing these findings. Future studies should include additional AML cell lines representing different molecular subtypes, as well as patient-derived primary cells, to validate the observed miRNA and mRNA expression patterns. Furthermore, functional assays using miRNA mimics/inhibitors or siRNA-mediated knockdown of key targets such as MYH9, ATM, and SOD2 are necessary to directly confirm their roles in radiation resistance. Such validations will be crucial for establishing the broader applicability and clinical relevance of our findings. Clinically, the identified miRNAs and their targets (e.g., MYH9, ATM, SOD2) may serve as biomarkers for predicting radiotherapy resistance in AML. They may also provide novel therapeutic targets to overcome such resistance, enabling more personalized treatment

strategies. Although our findings are currently preclinical, they lay important groundwork for future translational research aimed at improving AML patient outcomes.

In summary, further studies are warranted to clarify the role of these miRNA-mRNA networks in therapy-resistant leukemia. Future investigations employing integrative miRNA-mRNA analyses, as demonstrated here, may further elucidate the molecular basis of radiosensitivity in AML.

**Acknowledgements**

Not applicable.

**Funding**

This work was supported by JSPS KAKENHI, Grants-in-Aid for Scientific Research (B) (grant no. 21H02861/23K21419, to Satoru Monzen) and Takeda Science Foundation 2022 (to Satoru Monzen). The funders played no role in the study design, data collection and analysis, decision to publish, or preparation of the manuscript.

**Availability of data and materials**

The sequencing data generated in the present study may be found in the GEO under accession number GSE285934 or at the following URL: https://www.ncbi.nlm.nih.gov/geo/query/acc.cgi?acc=GSE285934. The other data generated in the present study may be requested from the corresponding author.

**Authors' contributions**

HS, YH and SM designed the study, prepared the manuscript draft and participated in the revision of the manuscript. HS, MK, MC and SM performed the biological analysis and collection of the experimental data. SM supervised the study, critically reviewed the manuscript and provided final approval for the version to be submitted and published. All authors have read and approved the final version of the manuscript. HS and SM confirm the authenticity of all the raw data.

**Ethics approval and consent to participate**

Not applicable.

**Patient consent for publication**

Not applicable.

**Competing interests**

The authors declare that they have no competing interests.

**References**

1. Nemkov T, D'Alessandro A and Reisz JA: Metabolic underpinnings of leukemia pathology and treatment. Cancer Rep (Hoboken) 2: e1139, 2019.
2. Shallis RM, Wang R, Davidoff A, Ma X and Zeidan AM: Epidemiology of acute myeloid leukemia: Recent progress and enduring challenges. Blood Rev 36: 70-87, 2019.
3. Wang ZY and Chen Z: Acute promyelocytic leukemia: From highly fatal to highly curable. Blood 111: 2505-2515, 2008.
4. Reske SN, Deisenhofer S, Glatting G, Zlatopolskiy BD, Morgenroth A, Vogg ATJ, Buck AK and Friesen C: 123I-ITdU-mediated nanoirradiation of DNA efficiently induces cell kill in HL60 leukemia cells and in doxorubicin-, beta-, or gamma-radiation-resistan cell lines. J Nucl Med 48: 1000-1007, 2007.
5. Godley LA and Larson RA: Therapy-related myeloid leukemia. Semin Oncol 35: 418-429, 2008.
6. Bhatia S: Therapy-related myelodysplasia and acute myeloid leukemia. Semin Oncol 40: 666-675, 2013.
7. Nemecek ER, Hilger RA, Adams A, Shaw BE, Kiefer D, Le-Rademacher J, Levine JE, Yanik G, Leung W, Talano JA, *et al*: Treosulfan, fludarabine, and low-dose total body irradiation for children and young adults with acute myeloid leukemia or myelodysplastic syndrome undergoing allogeneic hematopoietic cell transplantation: prospective phase II trial of the pediatric blood and marrow transplant consortium. Biol Blood Marrow Transplant 24: 1651-1656, 2018.
8. Monzen S, Takimura K, Kashiwakura I and Hosokawa Y: Acute promyelocytic leukemia mutated to radioresistance suppressed monocyte lineage differentiation by phorbol 12-myristate 13-acetate. Leuk Res 37: 1162-1169, 2013.
9. Hazawa M, Hosokawa Y, Monzen S, Yoshino H and Kashiwakura I: Regulation of DNA damage response and cell cycle in radiation-resistant HL60 myeloid leukemia cells. Oncol Rep 28: 55-61, 2012.
10. Monzen S, Chiba M, Ueno T, Morino Y, Terada K, Yamaya H and Hosokawa Y: A radioresistant fraction of acute promyelocytic leukemia cells exhibit CD38 cell-surface antigen and mRNA expression. Oncol Lett 15: 6709-6714, 2018.
11. Monzen S, Chiba M and Hosokawa Y: Genetic network profiles associated with established resistance to ionizing radiation in acute promyelocytic leukemia cells and their extracellular vesicles. Oncol Rep 35: 749-756, 2016.
12. Morino Y, Sugiyama H, Yamane K, Kikuchi M, Yamanaka T, Honda K and Monzen S: Additive antitumor effect of arsenic trioxide with exposure to ionizing radiation to human acute promyelocytic leukemia HL-60 cells. Oncol Rep 52: 109, 2024.
13. He B, Zhao Z, Cai Q, Zhang Y, Zhang P, Shi S, Xie H, Peng X, Yin W, Tao Y and Wang X: miRNA-based biomarkers, therapies, and resistance in cancer. Int J Biol Sci 16: 2628-2647, 2020.
14. Sun Z, Shi K, Yang S, Liu J, Zhou Q, Wang G, Song J, Li Z, Zhang Z and Yuan W: Effect of exosomal miRNA on cancer biology and clinical applications. Mol Cancer 17: 147, 2018.
15. Peng Y and Croce CM: The role of MicroRNAs in human cancer. Signal Transduct Target Ther 1: 15004, 2016.
16. Partida-Sánchez S, Cockayne DA, Monard S, Jacobson EL, Oppenheimer N, Garvy B, Kusser K, Goodrich S, Howard M, Harmsen A, *et al*: Cyclic ADP-ribose production by CD38 regulates intracellular calcium release, extracellular calcium influx and chemotaxis in neutrophils and is required for bacterial clearance in vivo. Nat Med 7: 1209-1216, 2001.
17. Livak KJ and Schmittgen TD: Analysis of relative gene expression data using real-time quantitative PCR and the 2(-Delta Delta C(T)) method. Methods 25: 402-408, 2001.
18. Mouly E, Planquette C, Rousseau E and Delansorne R: Inecalcitol enhances daratumumab-induced antibody-dependent cell cytotoxicity towards multiple myeloma and acute myeloid leukemia cell lines. Blood 132 (Suppl 1): S1447, 2018.
19. Zhong X and Ma H: Targeting CD38 for acute leukemia. Front Oncol 12: 1007783, 2022.
20. Breitman TR, Chen ZX and Takahashi N: Potential applications of cytodifferentiation therapy in hematologic malignancies. Semin Hematol 31 (4 Suppl 5): S18-S25, 1994.
21. Johansson P, Fasth A, Ek T and Hammarsten O: Validation of a flow cytometry-based detection of γ-H2AX, to measure DNA damage for clinical applications. Cytometry B Clin Cytom 92: 534-540, 2017.
22. Yuan W, Sun Q, Jiang Y, Zhang X, Chen L, Xie C, Qin F, Chen Y, Lv H, Chen W and Xiao Y: MiR-146a affects the alteration in myeloid differentiation induced by hydroquinone in human $CD34^+$ hematopoietic progenitor cells and HL-60 cells. Toxicol Res (Camb) 5: 848-858, 2016.
23. Vergani E, Dugo M, Cossa M, Frigerio S, Di Guardo L, Gallino G, Mattavelli I, Vergani B, Lalli L, Tamborini E, *et al*: miR-146a-5p impairs melanoma resistance to kinase inhibitors by targeting COX2 and regulating NFkB-mediated inflammatory mediators. Cell Commun Signal 18: 156, 2020.

24. Tse AKW, Wan CK, Shen XL, Zhu GY, Cheung HY, Yang M and Fong WF: 1,25-dihydroxyvitamin D3 induces biphasic NF-kappaB responses during HL-60 leukemia cells differentiation through protein induction and PI3K/Akt-dependent phosphorylation/degradation of IkappaB. Exp Cell Res 313: 1722-1734, 2007.
25. Zhang X, Zhang G, Huang H, Li H, Lin S and Wang Y: Differentially expressed MicroRNAs in radioresistant and radiosensitive atypical meningioma: A clinical study in chinese patients. Front Oncol 10: 501, 2020.
26. Chen W, Yao G and Zhou K: miR-103a-2-5p/miR-30c-1-3p inhibits the progression of prostate cancer resistance to androgen ablation therapy via targeting androgen receptor variant 7. J Cell Biochem 120: 14055-14064, 2019.
27. Lin JC, Kuo CY, Tsai JT and Liu WH: miR-671-5p inhibition by MSI1 promotes glioblastoma tumorigenesis via radioresistance, tumor motility and cancer stem-like cell properties. Biomedicines 10: 21, 2021.
28. Qiu X and Qin F: Retraction: FAM64A antagonizes tumor suppressive effects of miR-610 in neuroblastoma in vitro. J Neurosurg Sci: Apr 16, 2021 (Epub ahead of print).
29. Liu Y, Hu L, Liu O, Ye J and Zhang J: miR-3651 participates in the growth cycle of hepatocellular carcinoma cells and promotes the malignant metastasis via the PI3K/AKT/mTOR signalling pathway. J Oncol 2022: 5744999, 2022.
30. Li C, Ding D, Gao Y and Li Y: MicroRNA-3651 promotes colorectal cancer cell proliferation through directly repressing T-box transcription factor 1. Int J Mol Med 45: 956-966, 2020.
31. Noh JK, Woo SR, Yun M, Lee MK, Kong M, Min S, Kim SI, Lee YC, Eun YG and Ko SG: SOD2- and NRF2-associated gene signature to predict radioresistance in head and neck cancer. Cancer Genomics Proteomics 18: 675-684, 2021.
32. You GR, Chang JT, Li YL, Huang CW, Tsai YL, Fan KH, Kang CJ, Huang SF, Chang PH and Cheng AJ: MYH9 facilitates cell invasion and radioresistance in head and neck cancer via modulation of cellular ROS levels by activating the MAPK-Nrf2-GCLC pathway. Cells 11: 2855, 2022.
33. Yu M, Wang J, Zhu Z, Hu C, Ma Q, Li X, Yin X, Huang J, Zhang T, Ma Z, *et al*: Prognostic impact of MYH9 expression on patients with acute myeloid leukemia. Oncotarget 8: 156-163, 2017.
34. Metzeler KH, Hummel M, Bloomfield CD, Spiekermann K, Braess J, Sauerland MC, Heinecke A, Radmacher M, Marcucci G, Whitman SP, *et al*: An 86-probe-set gene-expression signature predicts survival in cytogenetically normal acute myeloid leukemia. Blood 112: 4193-4201, 2008.
35. Zhai Y, Shen H and Wei H: A comprehensive metabolism-related gene signature predicts the survival of patients with acute myeloid leukemia. Genes (Basel) 15: 63, 2023.
36. Gregory MA, D'Alessandro A, Alvarez-Calderon F, Kim J, Nemkov T, Adane B, Rozhok AI, Kumar A, Kumar V, Pollyea DA, *et al*: ATM/G6PD-driven redox metabolism promotes FLT3 inhibitor resistance in acute myeloid leukemia. Proc Natl Acad Sci USA 113: E6669-E6678, 2016.